2020 IEEE/RSJ International Conference on Intelligent Robots and Systems (IROS)
October 25-29, 2020, Las Vegas, NV, USA (Virtual)

Magnetically Actuated Pick-and-place Operations of Cellular Micro-rings for High-speed Assembly of Micro-scale Biological Tube

Yang Wu, Tao Sun, *Member, IEEE,* Qing Shi, *Member, IEEE,* Huaping Wang, *Member, IEEE,* Qiang Huang, *Fellow, IEEE* and Toshio Fukuda, *Fellow, IEEE*

***Abstract*— Tissue engineering is trying to use modular tissue micro-rings to construct artificial biological microtubes as substitute of autologous tissue tubes to alleviate the shortage of donor sources. However, because of the lack of effective assembly strategies, it is still challenging to achieve high-speed fabrication of biological microtubes with high cell density. In this paper, we proposed a robotic-based magnetic assembly strategy to handle this challenge. We first encapsulated magnetic alginate microfibers into micro-rings formed by cell self-assembly to enhance the controllability. Afterwards, a 3D long-stroke manipulator with visual servoing system was designed to achieve magnetic pick-and-place operations of micro-rings for 3D assembly. Moreover, we developed a mathematical model of the motion of micro-ring in solution environments. Based on visual feedback, we analyzed the feasibility of automatic assembly and following response of micro-rings with the moving magnets, which shows our proposed method has great potential to achieve high-speed bio-assembly. Finally, we successfully assembled multi-micro-rings into a biological microtube with high cell density.**

I. Introduction

In human body, biological tubes take a critical role of transporting gases, liquid, such as blood vessels, tracheas, et al [1]. The collapse of biological tubes may cause the failure of the circulation of the human that could quickly become life-threatening. Based on traditional treatment strategy of transplantation, the damaged tubes can be replaced by a variety of tube substitutes [2-3]. However, the present tube substitutes exists several serious problems, including the limited supply sources, the lack of ideal substitutes with biologically and morphologically relevant functions, and the immunological rejection, et al [4].

For trying to solve these problems, tissue engineering is developing a "bottom-up" construct method to assemble tissue rings into artificial biological tubes, microtubes in particular because the majority of natural biological tubes are small and their size is in the order of microns [5]. On the basis of the fabrication method, the existing tissue micro-rings can be categorized into two types: cell-encapsulated hydrogel micro-rings and self-assembling cell micro-rings [6-7]. For hydrogel micro-rings, hydrogels can provide a stable protective shell for the encapsulated cells, which enables multiple 3D microtube-like assembly methods to be developed by utilizing capillary force, flowing liquid, robotic manipulators and magnetic force, et al [8-11]. However, the hydrogel shell may induce inhomogeneous cell distribution, and inevitably hinder the process of cell compaction, which causes the resulting microtubes to difficultly form high cell density similar with cell density of human organs [12].

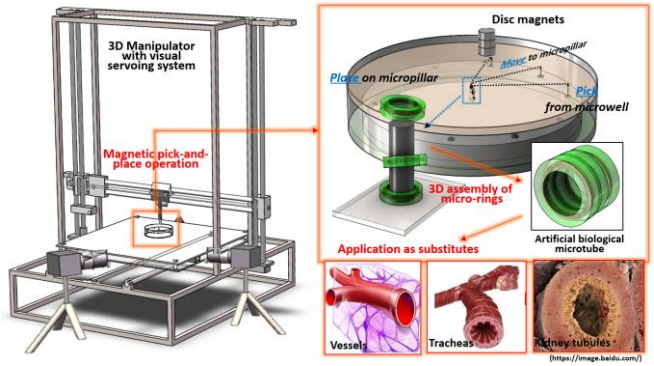

Fig. 1 A schematic drawing of robotic-based magnetic assembly of biological microtube and its application in tissue engineering.

Annular wells on nonadhesive hydrogels provide a well-established platform to facilitate self-assembly of cells into tissue rings with high cell density [13]. To further use tissue rings as building blocks to create tissue tubes, the rings should be removed from wells, transferred to tube mandrels. Because the size of rings were a few millimetres in previous works [14-15], such transfer was easy to be operated manually. When the size of rings was at the microscale, unstable manual operation greatly increased the risk of damaging micro-rings. Compared with manual assembly, robotic assembly was better for microassembly because of its high precision and stability. For robotic manipulation, unmanageable operating force applied by rigid end-effectors is suitable for only gels-protected tissue modules rather than hydrogel-free cell micro-rings [16-17]. Magnetic manipulation can provide a gentler operating force relative to robotic manipulation for cellular micro-objects. Professor M. Sitti developed a representative work to use an untethered magnetic microstructure remotely controlled by magnetic field to achieve bottom-up assembly [18-20]. Such non-contact manipulation method can effectively avoid the irreversible damages and potential contamination in the assembly process [21-23]. However, the expensive peripheral magnetic coil system and complex control method seriously limit its wide application in tissue engineering. Therefore, a more common magnetic assembly method should be further developed.

* This work was supported by the National Key R&D Program of China under grant no. 2017YFE0117000 and the National Nature Science Foundation of China (NSFC) under Grant 61703045

T. Sun is with Beijing Advanced Innovation Center for Intelligent Robots and Systems, Beijing Institute of Technology, Beijing 100081, China, (e-mail: 3120120061@ bit.edu.cn).

Y. Wu, Q. Shi, HP Wang, Q. Huang and T. Fukuda are with the Intelligent Robotics Institute, Key Laboratory of Biomimetic Robots and system, Ministry of Education, School of Mechatronical Engineering, Beijing Institute of Technology, Beijing 100081, China

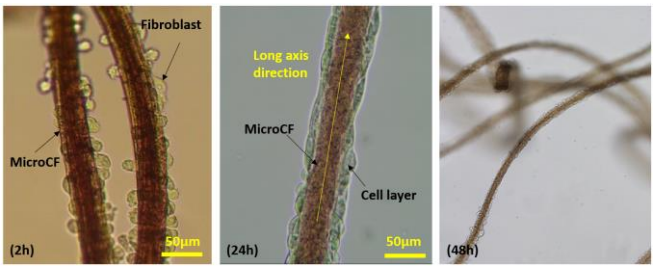

Fig. 2 Time-lapse images of cell growth on microCFs.

In this paper, we proposed a simple, cheap, but efficient magnetic manipulation method for high-speed assembly of self-assembling cell micro-rings, as show in Fig. 1. Magnetic alginate microfibers were involved in the process of cell self-assembly to form micro-rings with a strong response for external magnetic field. In solution environment, the moving space of micro-ring could be bounded by the interface of air and solution. For simplicity, we utilized the interface to provide the position control of micro-rings in z direction. Multiple micro-rings were simultaneously fabricated on an agarose platform. For economy, a common 3D printer was converted into a robotic system with a large stroke, which enabled the installed magnet to arrive any location on the agarose platform for collecting micro-ring. For efficiency, the visual servoing can be involved, and the strategy of automatic assembly was investigated. Based on these features, a potential feasibility of high-speed bio-assembly was presented in detail.

II. Fabrication of Tissue Micro-rings Incorporating Magnetic Hydrogel Microfibers

A. Microfluidic synthesis of magnetic alginate microfibers with cell adhesion sites

The powders of Fe_3O_4 magnetic nanoparticles (MNPs) (0.05g) were uniformly dispersed into 1.25% (w/v) alginate solution (10mL). Based on multi-laminar spinning system, the alginate solution was transferred into alginate hydrogel microfibers, and the encapsulated MNPs enabled the microfibers to have a rapid response for external magnetic field. To increase cell adhesion sites, a surface modification procedure was implemented by successively coating Poly-L-Lysine (0.01mg/mL) and Fibronectin (10μg/ml) on microfiber surface. Subsequently, NIH/3T3 fibroblasts were directly seeded on the top of the coated microfibers (microCFs). Initially, cells with spherical morphology spontaneously attached onto microCFs. After 24h of culturing, cells elongated along microCFs and connected with each other. With the continuous secretion of extracellular matrix (ECM), a semi-transparent cellular layer was formed, as shown in Fig. 2. In additional, microfiber-dependent cellular alignment could be engineered, and cells were orientated to spread along the long axis of microCFs.

B. Fabrication of microCFs-incorporated tissue micro-rings based on annular agarose microwells

Based on molding method, 10 annular microwells were processed on the surface of circle agarose platform. For connecting the platform with a culture dish, an agarose stationary barrier was filled into the gap between the platform and the dish. The dish was placed on the surface of a

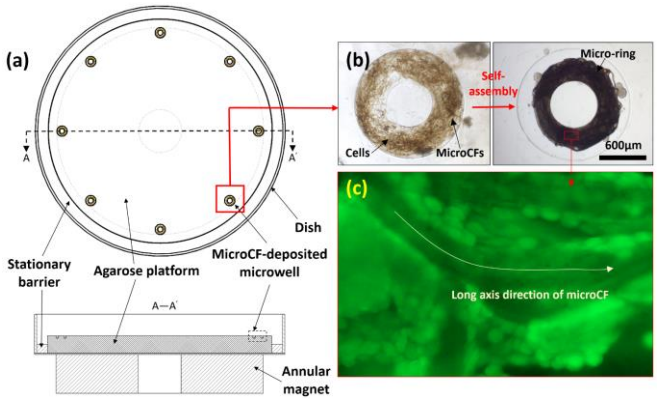

Fig. 3 Fabrication of tissue micro-rings encapsulating microCFs. (a) Agarose platform. (b) Self-assembly of cells and microCFs to form tissue micro-rings. (c) Cell alignment along long axis direction of microCFs in micro-ring.

neodymium ring magnet, and microCFs were magnetically deposited and annularly arranged in the microwells. Otherwise, microCFs usually floated into cell culture solution. The overall architecture was shown in Fig.3a. The round bottoms of the microwells facilitated cell self-aggregation. When fibroblasts suspension was seeded into the microwells, fibroblasts could initially spread on microCFs. Based on the further spreading over different microCFs, all microCFs could be connected by fibroblasts after ~ 24 h of culture. Afterwards, microCFs could follow the self-assembly of fibroblasts to be assembled together, and a tissue micro-ring was finally formed, as shown in Fig. 3b. The encapsulated microCFs not only showed the potential of controlling over cell alignment in the micro-rings (Fig. 3c), but also enabled the micro-rings to be moved towards external magnetic field.

III. Magnetically Actuated Pick-and-Place Operations of Tissue Micro-rings

A. Operation system step

The operation system was composed of a 3-DOFs manipulator modified from a simple 3D printer, disc magnets, the agarose platform containing tissue micro-rings, and two side-view microscopes monitoring the assembly process, as shown in Fig. 4. Disc magnets (B_{max}=0.4T, diameter: 3mm) was vertically installed under the slider of the manipulator. Depending on pulley and lead screw drive, the slider enabled the magnets to move along X and Z direction with a positioning resolution of 0.01mm and 0.004mm, respectively. The agarose platform was placed on the center of the mobile platform of the manipulator, which enabled the platform to be moved along Y direction with a positioning resolution of 0.01mm. Moreover, a copper micro-pillar (diameter: 0.4mm) was vertically inserted into the center of the agarose platform to provide structural support for the subsequent assembly, and the segment length of micro-pillar for the assembly is 3mm.

Two side views were established by employing two industrial cameras for 3D real-time localization of micro-ring and disc magnets. Camera 1 with normal lens and Camera 2 with microscope lens were placed in two directions perpendicular to each other. Because of the extremely short picking time of micro-ring, we used a high-speed CMOS camera as Camera 2 which had a maximum frame rate (f_{max}=136 fps). The 3D manipulator and two cameras were connected together to a master computer. When the system

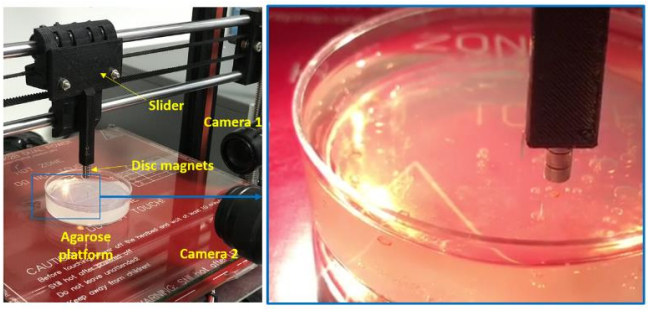

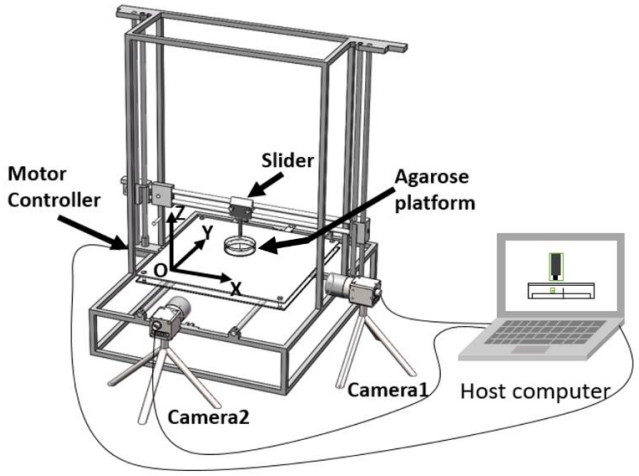

Fig. 4 Operation system for 3D assembly of micro-rings

was enabled, the captured source images were sent to the master computer. After processing source images, tracking and localization algorithms were performed to get the real-time position information of micro-rings and the magnets. These position information were used as inputs of the visual feedback to further control motor controller to manipulate the magnets

B. *Pick-and-place operation mechanism and mathematical model of the motion of tissue micro-ring in liquid environment*

Contactless pick-and-place operation of micro-rings were performed by descending-and-lifting of the magnets, as shown in Fig. 5. When the magnets approached, micro-ring was picked up because of upwards magnetic attraction, and then such pick-up process was terminated by the interface of air and solution. The picked micro-ring located on the low surface of the interface could follow the movement of the magnets, which enabled the centre of the micro-ring to be aligned with the micropillar. Afterwards, the lifted magnets released the micro-rings from the interface, and the micro-ring relied on gravitation to deposit to be placed into micropillar. Considering the movement of micro-rings in X-direction, and the effects of gravity and buoyancy were ignored, we developed following mathematical model to describe the motion of micro-ring, according to Newton's Second Law:

$$m\ddot{x} = [F_m(x', h)]_x - F_d(\dot{x}) \quad (1)$$

Where F_m was magnetic force which was exerted on the picked micro-ring by the magnets, F_d was the drag force which is exerted by liquid environment. The first term was the inertia force on the micro-ring. Here, the dependent parameters are velocity ($\dot{x}$(t)) and acceleration ($\ddot{x}$(t)), h is the

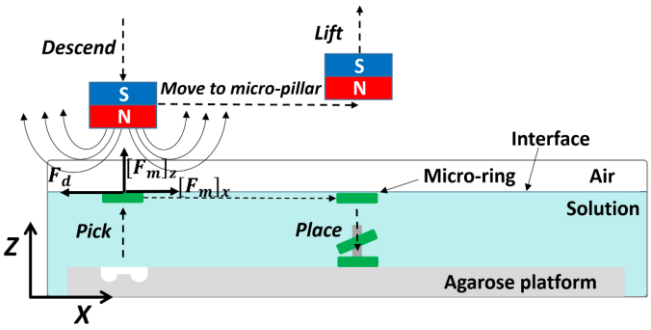

Fig. 5 Schematic drawing of pick-and-place operations of micro-ring

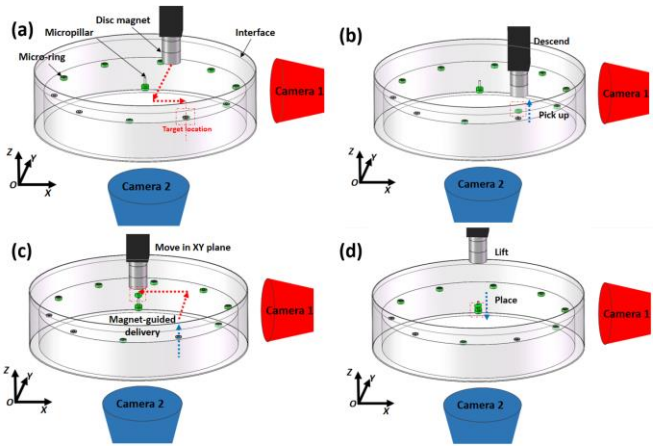

Fig. 6 Magnetically guided assembly strategy.(a) Locating magnets to targeted micro-ring. (b) Descending magnets to pick up micro-ring. (c) Moving magnets to deliver micro-ring on the micropillar (d) Placing micro-ring with lifting of magnets.

vertical height of the magnets from the micro-ring in z-direction, x' is relative position of the magnets with the micro-ring:

$$x' = V_m t - x(t) \quad (2)$$

Where V_m was the velocity of the magnet, $x(t)$ was position of the micro-ring in x-direction.

Because the size of the micro-ring was so small that the vortex effect was not obvious, we used the "linear damping term" to describe drag force. The drag force exerted by the liquid environment was expressed as:

$$F_d = 6\pi\eta r\dot{x} \quad (3)$$

In which, η was the viscosity of culture solution, and r was radius of micro-ring, $\dot{x}$ was the velocity of micro-ring.

Considering that micro-ring was a homogenous medium since the powders of Fe_3O_4 magnetic nanoparticles were uniformly dispersed into the micro-ring, we described the magnetic force in the volume of the micro-ring as:

$$\overrightarrow{F_m} = \iiint_v (\nabla \times \vec{M}) \times \vec{B}\, dv \quad (4)$$

Where, $\vec{B}$ and $\vec{M}$ were the magnet flux density and magnetization at the location of the micro-ring, respectively. $\vec{M}$ could be expressed as:

$$M = \frac{\mu_r - 1}{\mu_r \mu_0} B \quad (5)$$

μ_r was relative permeability of magnetic media, μ_0 was the vacuum permeability.

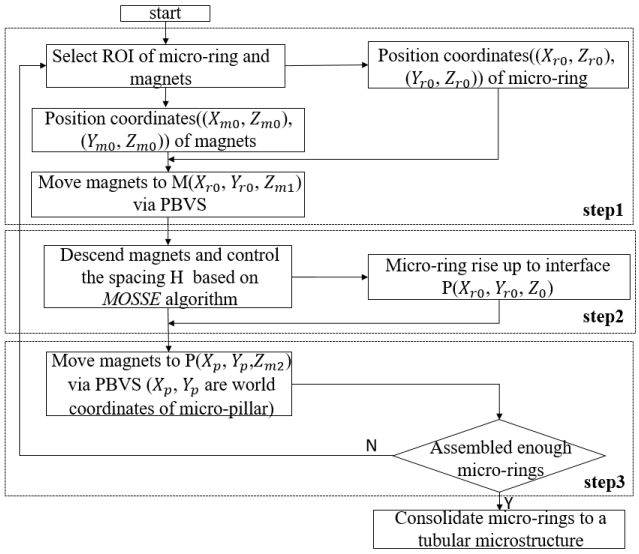

Fig. 7 Flow chart of assembling micro-rings with visual feedback

The Equation (5) was substituted into (4), and after vector operation we obtain the magnetic force as follow:

$$\overrightarrow{F_m} = \frac{\mu_r - 1}{2\mu_r\mu_0} \iiint_v \nabla \cdot \vec{B}^2 dv \tag{6}$$

Furthermore, it was possible to simplify the magnetic force, according to the Gauss's divergence theorem, we obtained magnetic force in the surface of the micro-ring as:

$$F_m = \frac{\mu_r - 1}{2\mu_r\mu_0} \oiint_S B^2 dS \tag{7}$$

Substituting equation (7) and (3) into Equation (1), we could obtained final model equation describing x-direction motion of the micro-ring:

$$m\ddot{x} = \frac{\mu_r - 1}{2\mu_r\mu_0} \oiint_S B^2 dS \cdot \cos\theta - 6\pi\eta r\dot{x} \tag{8}$$

Where $\theta = \tan^{-1} h/x'$.

IV. Magnetic Assembly of Tissue Micro-rings to Biological Microtube

A. Assembly strategy based on two cameras

The manipulator enabled the magnets to move in X, Y, Z direction to three-dimensionally pick and place micro-rings. Multi-micro-rings could be successively assembled on the micropillar. Furthermore, based on the visual feedback system, we could try to implement an automated operation to achieve high-speed assembly.

There are two cameras arranged vertically, Camera 1 and Camera 2 are used to capture the real-time position and motion information of the target in Y, Z, and X, Z directions, respectively. When the system was enabled, we firstly switched to camera 1 to obtain the source image and select the initial position (ROI) of the micro-ring (Y_{r0}, Z_{r0}) and magnets (Y_{m0}, Z_{m0}) in the first frame, then performed real-time tracking on subsequent frames. Based on the real-time position estimation, we could manipulate magnets to a new position having the world coordinate (Y_{r0}, Z_{m1}) (where $Z_{m1} >> Z_{r0}$). Afterwards, we switched to Camera 2 and use the subsequent first frame as the initial frame for object tracking, and selected the initial position of the magnets (X_{m0}, Z_{m1}) and

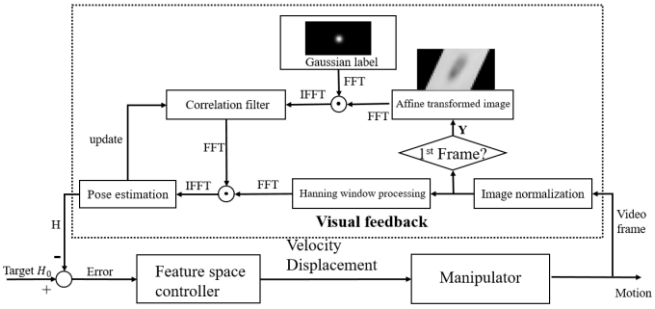

Fig. 8 Position based visual servoing for controlling spacing H

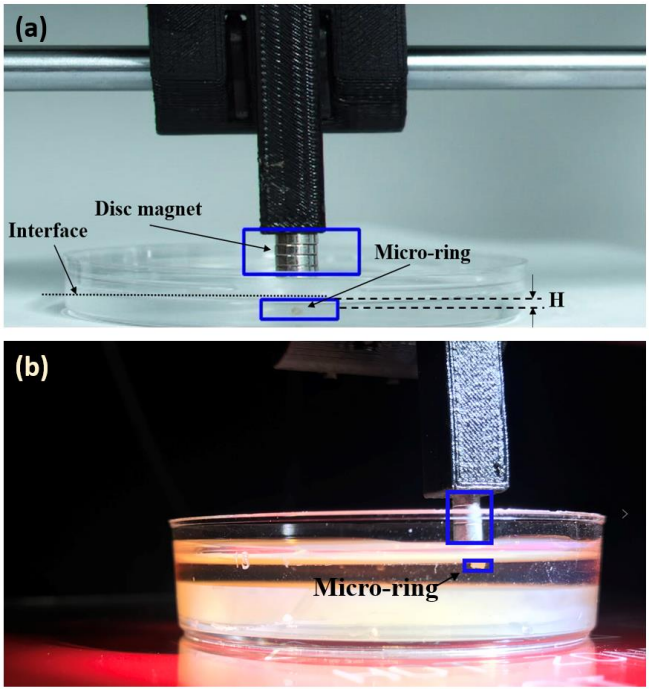

Fig. 9 Real-time tracking position of micro-ring and magnets based on MOSSE algorithm. (a) Image from Camera 2 for motoring the pick-up of micro-ring, (b) Image from Camera 1 for guiding the movement of magnets to deliver micro-ring on micropillar.

micro-ring (X_{r0}, Y_{r0}) in the X, Z directions. Then we manipulated magnets to a position having the world coordinate (X_{r0}, Y_{r0}, Z_{m1}), subsequently descended the magnets to position M (X_{r0}, Y_{r0}, Z_{m2}) so that micro-ring could be attracted by magnets and rise to the interface between air and solution. Benefiting from enough interval distance between adjacent microwells, the picked micro-ring was limited to the only microwell over which the magnets move, while micro-rings in the neighbouring microwells were not disturbed. After confirming the arrival of micro-ring to the interface, we then controlled the movement of micro-ring by manipulating magnets and switching to Camera 1 and Camera 2 in sequence, and finally manipulated magnets to positon P(X_p, Y_p, Z_{m2}) (where X_p, Y_p are world coordinates in X and Y direction of the micropillar, respectively). After picking up the magnets in Z direction, the micro-ring was released by gravity, and it could be strung by micro-pillar. The placing process was motored by the Camera 2. Because of the long-stroke provided by the manipulator, the pick-and-place process was repeated from different microwells, and micro-rings were magnetically stacked one by one. The whole assembly process was shown in Fig. 6 and Fig. 7.

B. *Real-time visual servoing for pick-and-place operation*

In view of the extremely short pick-up process of micro-ring, MOSSE algorithm was used to achieve real-time visual servo control, as shown in Fig. 8. The MOSSE algorithm based on correlation filter takes grayscale features as input information and has high accuracy and real-time tracking performance. Because of the obvious grayscale characteristics of micro-ring and magnet under a specially designed illumination, MOSSE algorithm was well implemented in magnetic assembly process

We used the Camera 2 to motor the pick-up process (Fig. 9a). In this process, an appropriate distance H should be kept between the micro-ring and the magnet, otherwise, too small H might cause the micro-ring to be pulled out of the solution through the interface. According to the actual measurement, we found that micro-ring could be stably picked up when H was in a distance range (h_{min} < H < h_{max} , where $h_{min} \cong 2mm$, $h_{max} \cong 6mm$). Visual servo could automatically facilitated the maintenance of such H, when the distance between the micro-ring and the magnet was less than h_{min}, as shown in Video S1. Afterwards, we switched to the Camera 1 to guide the magnets to be moved onto the micropillar, and then the center of micro-ring was just aligned to the micropillar, as shown in Fig. 9b and Video S2. (For presenting the whole moving process, Video S2 was recorded by handheld camera rather than Camera 1). However, the success rate of such alignment was low since there was lack of real-time relative position feedback between centre point of the micro-ring and top point of the micropillar. In future, we will solve this problem by adjusting the motoring angle of the Camera 1[24-26].

C. *Following response of micro-ring actuated by magnet*

The velocity of the magnet could affect the following movement of micro-ring. Specifically, when the magnet moved at high velocity, micro-ring might fail to follow with magnet. Hence, in order to implement high-speed robotic assembly of micro-rings, it is necessary to quantitatively analyze the following response of micro-ring with magnet.

By using Camera 2 with normal lens, we performed object detection analysis on micro-ring and magnet based on video frames input. Since the following movement of micro-ring changes rapidly, we set the acquisition frame rate of high-speed camera to be approximately constant at 100fps. Firstly, we performed Gaussian filtering and image binarization on the source image for reducing image noise. Afterwards, we performed motion detection algorithm by using background segmentation method, as shown in Fig. 10a. Then, we got center pixel coordinates of micro-ring and magnet at different time with template marching and moment marching. To get the world coordinates of micro-ring and magnet, camera calibration was performed as shown in Fig. 10b. The displacement of micro-ring and magnet at different time are shown in Fig. 11. The origin of coordinates was set at the starting position of motion.

From these experiment result, it could be concluded that there exist an extreme velocity V_e between 1800-2000mm/min for the magnet to enable the micro-ring to follow with it. To ensure that micro-ring can keep up with magnet, we should

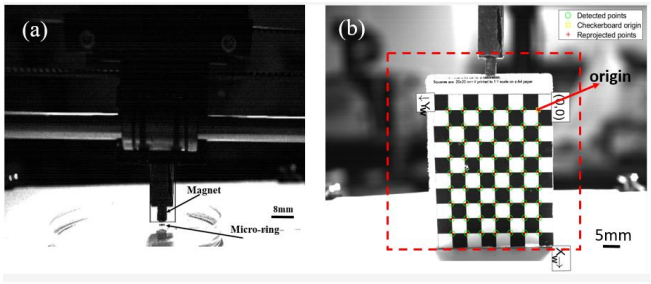

Fig. 10 (a) Motion detection and tracking. (b) Camera calibration

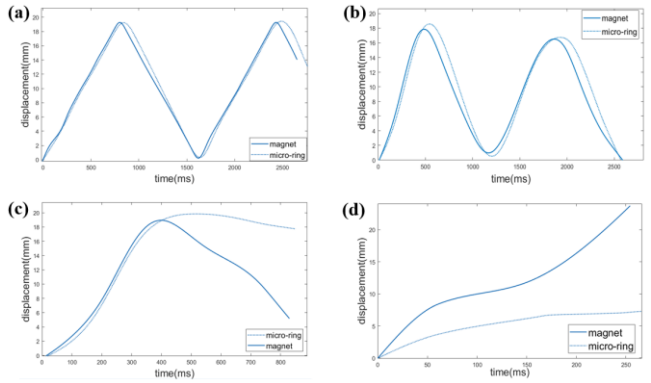

Fig. 11 Following response of micro-ring with magnet when velocity of magnet at (a) 1500mm/min, (b) 1800mm/min, (c) 2000mm/min. (d) 2500mm/min.

restrict velocity of magnet to a value less than the extreme velocity V_e which exists in the range of 1800-2000mm/min.

D. *Formation of tubular microstructure*

Based on the above-mentioned assembly strategy, we could preliminarily achieve the successive assembly of micro-rings. There are two key steps require to be especially explained. First, Cell traction force always fixed microTRs on the micropost of microwells, which prevented microTRs from being magnetically levitated. However, the agarose microposts (diameter: 600μm) were so soft that they could be severely deformed by light pressure. Therefore, we used a copper wire with diameter of 400μm to press the micropost under a magnifying glass. The microposts were first destroyed, and then the miroTRs were levitated when magnetic disc moved over the microwell. Second, when the magnet approached micropillar, the assembled micro-ring tilted because a moment of magnetic force occurred. The moment could generate the friction of micro-ring against micropillar, which could effectively prevent the assembled micro-rings form escaping from the micropillar. Therefore, the assembly process was successively implemented. Cell fusion allowed the stable connection of the stacked micro-rings within 5 days of culture. After being released from the micropillar, a biological microtube was formed, as shown in Fig. 12b.

Although we have implemented the 3D assembly of micro-ring by controlling the movement of manipulator based on visual feedback system, there are still some problems need to be further solved. Because the switch between different cameras involves the switch between different threads of the same process in the program, and this operation often causes

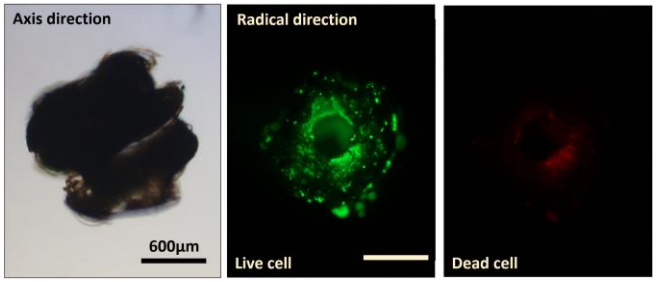

Fig. 12 Formation of biological microtube. Bright-field image of biological microtube; the corresponding fluorescent images of live cells from vertical view. Green color representing live cells, and red color indicating dead cells.

thread blocking and eventually causes the program to crash, in the future, it needs to be improved to implement smooth automatic camera switching. Since the initial positions of the magnets and tissue micro-rings need to be located for subsequent object tracking each time the camera is switched in the sub-process of assembly, it is necessary to develop an automatic detection method in the future to achieve automatic positioning of the initial position, and finally complete automatic assembly.

V. Conclusion

In this paper, we preliminarily developed a visual-based robotic system for the fabrication of biological microtubes. To reduce the risk of damaging micro-ring, we employed magnetically actuated method to assemble micro-rings via non-contact magnetic force. We established a mathematical model of the motion of micro-ring, and a quantitative analysis of following response of micro-ring with magnet was performed. The critical velocity range of magnet was concluded, which provided the references for the relatively rapid delivery of micro-rings without the risk of failing to follow with magnet. We also employed a position-based visual servoing approach to try to achieve automatic pick-and-place operation of micro-rings. Finally, we successfully obtained tubular microstructure via our magnetic assembly strategy. Because of the incorporation of visual servoing and simple assembly strategy, our method have a great potential to achieve a high-speed bio-assembly, which is significant for organs regeneration with a high cell bioactivity. In future, we will further develop the automatic process of such assembly method.

References

[1] B. Lubarsky and M. A. Krasnow. "Tube morphogenesis: making and shaping biological tubes, " *Cell*, vol. 112, no. 1, pp:19-28, JAN, 2003.

[2] Y. M. Ju, H. Ahn, J. Arenas-Herrera, et al. "Electrospun vascular scaffold for cellularized small diameter blood vessels: a preclinical large animal study," *Acta Biomater*, vol. 59, pp:58-67, SEP, 2017.

[3] H. C. Grillo. "Tracheal replacement: a critical review," *Ann. Thorac. Surg*, vol. 73, no. 6, pp:1995-2004, JUN, 2002.

[4] E. J. Ten Hallers, G. Rakhorst, H. A. Marres, et al "Animal models for tracheal research," *Biomaterials*, vol. 25, no. 9, pp:1533-1543, APR, 2004.

[5] J. W. Nichol and A. Khademhosseini "Modular tissue engineering: engineering biological tissues from the bottom up," *Soft. Matter*, vol. 5, no. 7, pp:1312-1319, 2009.

[6] H. P. Wang, J. Cui, Z. Q. Zheng, et al. "Assembly of RGD-modified hydrogel micromodules into permeable three-dimensional hollow microtissues mimicking in vivo tissue structures," *ACS. Appl. Mater. Inter*, vol. 9, no. 48, pp:41669-41679, DEC, 2017.

[7] W. G. Yang, H. B. Yu, G. X. Li, et al "Mask-free fabrication of a versatile microwell chip for Multi-dimensional cellular analysis and drug screening," *Lab. Chip*, vol. 17, no. 24, pp:4243-4252, DEC 2017.

[8] Y. Du, M. Ghodousi, E. Lo, et al "Surface-Directed Assembly of Cell-Laden Microgels," *Biotechnol. Bioeng.*, vol. 105, no. 3, pp:655-662, FEB 2010.

[9] T. Yue, M. Nakajima, M. Takeuchi, et al "Fluidic self-assembly of multilayered tubular microstructures by axis translation inside two-layered microfluidic devices," *Proc. Of the 2014 IEEE Int. Conf. on Robotics and Automation (ICRA2014),* pp:5836-5841, 2014.

[10] H. Wang, Q. Shi, T. Yue, et al "Micro-assembly of a vascular-like micro-channel with railed micro-robot team-coordinated manipulation," *Int. J. Adv. Rob. Syst.,* vol. 11. 115. JUL, 2014.

[11] S. E. Chung, X. G. Dong, M. Sitti. "Three-dimensional heterogeneous assembly of coded microgels using an untethered mobile microgripper," *Lab. Chip,* vol. 15, no. 7, pp:1667-1676. 2015

[12] H. J. Kong, E. Alsberg, D. Kaigler, et al. "Controlling degradation of hydrogels via the size of crosslinked junctions," *Adv. Matter,* vol. 16, no. 7, pp:1917-1921. 2004.

[13] O. Adebayo, T. A. Hookway, J. Z. Hu, et al. "Self-assembled smooth muscle cell tissue rings exhibit greater tensile strength than cell-seeded fibrin or collagen gel," *J. Biomed. Mater. Res. A,* vol. 101, no. 7, pp: 428-437. 2013.

[14] A. Leferink, D. Schipper, E. Arts, et al. "Engineered micro-objects as scaffolding elements in cellular building blocks for bottom-up tissue engineering approaches," *Adv. Mater,* vol. 26, no. 9, pp: 2592-2599. MOV, 2014.

[15] T. A. Gwyther, J. Z. Hu, A. G. Christakis, et al. "Engineered vascular tissue fabricated from aggregated smooth muscle cells," *Cells. Tissues. Organs,* vol. 194, no. 3, pp: 13-24. SEP, 2011.

[16] X. M. Liu, Q. Shi, H. P. Wang, et al. "Automated fluidic assembly of microvessel-like structures using a multimicromanipulator system," *IEEE/ASME. Trans. Mech.,* vol. 23, no. 3, pp: 667-678. NOV, 2018.

[17] H. P. Wang, Q. Huang, Q. Shi et al. "Automated assembly of vascular-like microtube with repetitive single-step contact manipulation," *IEEE/ASME. T. BIO-MED. ENG,* vol. 62, no. 11, pp: 2620-2628. NOV, 2018.

[18] S. Tasoglu, E. Diller, S. Guven, et al. "Untethered micro-robotic coding of three-dimensional material composition," *NAT. COMMUN,* vol. 5, 3124, JAN, 2014.

[19] E. Diller, J. Giltinan, M. Sitti. "Independent control of multiple magnetic microrobots in three dimensions," *INT. J. ROBOT. RES,* vol. 32, no. 5, pp:614-631, APR, 2013.

[20] C. Pawashe, S. Floyd, E. Diller, et al. "Two-Dimensional Autonomous Microparticle Manipulation Strategies for Magnetic Microrobots in Fluidic Environments," *IEEE. T. ROBOT,* vol. 28, no. 2, pp:467-477, APR, 2012.

[21] M. Savia, H. N. Koivo, "Contact Micromanipulation-survey of Strategies," *IEEE/ASME. Trans. Mech*, vol.14, no. 4, pp: 504-514, Oct, 2009.

[22] M. Hagiwara, T. Kawahara, Y Yamanishi, et al, "On-chip Magnetically Actuated Robot with Ultrasonic Vibration for Single Cell Manipulation," *Lab. Chip*, vol. 11, no. 11, pp:2049-2054, Mar, 2011.

[23] A. H. B. D. Vries, B. E. Krenn, J. S. Kanger, et al, "Micro Magnetic Tweezers for Nanomanipulation Inside Live Cells," *Biophysical Journal*, vol. 88, no. 3, pp:2137-2144, Mar, 2005

[24] X. Yu, M. Jacob, S. Vincent, et al, "Optimization of Force Produced by Electromagnet Needles Acting on Superparamagnetic Microparticles," *Applied Physics Letter*, vol. 92, 124104, Aug, 2008

[25] Y. Chen, R. Xia, Q. Zhang, et al, "The visual object tracking algorithm research based on adaptive combination kernel," *Journal of Ambient Intelligence and Humanized Computing*, pp:1-13, 2019.

[26] F. Lin, H. Wei, Y. Qi et al, "Scale Adaptive Target Tracking Algorithm Based on Correlation Filtering," *Journal of Physics conference series,* 1284:012061, 2019.